

VENTRICULAR FUNCTION

Effects of Phase Encode Order and Segment Interpolation Methods on the Quality and Accuracy of Myocardial Tags During Assessment of Left Ventricular Contraction

Tiffany B. Salido,¹ W. Gregory Hundley,^{2,3} Kerry M. Link,^{2,3} Frederick H. Epstein,⁴ and Craig A. Hamilton^{1,*}

Departments of ¹Medical Engineering, ²Internal Medicine, and ³Radiology, Wake Forest University School of Medicine, Bowman Gray Campus, Medical Center Blvd., Winston-Salem, NC 27157

⁴Department of Radiology, University of Virginia School of Medicine, Charlottesville, VA 22908

ABSTRACT

Tissue tagging can be implemented during cardiovascular magnetic resonance imaging exams to assist with the quantification of left ventricular geometry, volume and ejection fraction, endocardial thickening and relaxation, and myocardial stress–strain relationships. During tagged cine gradient echo image acquisitions of left ventricular wall motion, rows of k-space data can be acquired with various phase-encoding orders, and the reconstruction of supplemental images can be accomplished using a variety of interpolation techniques. In this study, we investigated the utility of various phase order and segment interpolation methods for determining accurate tag displacement trajectories. Center-out phase order image acquisition with reconstruction using linear interpolation provided the highest tag position and displacement accuracy. Therefore, it is recommended that myocardial tagging exams be acquired with center-out phase encode order and reconstructed using linear segment interpolation when used for performing quantitative analysis of cardiovascular structure and function.

Key Words: *Magnetic resonance imaging; Myocardial tagging; Segmented k-space; Phase order*

*Corresponding author. Fax: (336) 716-2870; E-mail: crhamilt@wfubmc.edu

INTRODUCTION

Magnetic resonance imaging (MRI) tissue tagging is used to quantify left ventricular regional endocardial thickening and relaxation, as well as stress and strain (1–5). Often, submillimeter changes in these measurements (6,7) convey important clinical information regarding left ventricular remodeling, viability, or myocardial ischemia (8,9). For this reason, the precise location of the tags throughout the cardiac cycle must be known.

During tagged, breath-held, cine gradient echo acquisitions of the left ventricle (LV) (10,11), rows of k-space data can be acquired in various phase encode orders (PO). In addition, rows within segments acquired at adjacent times can be shared to reconstruct additional images using a variety of interpolation techniques, also referred to as view-sharing (12,16). The acquisition PO and the method of segment interpolation during reconstruction affects the appearance and position of the tags on the resultant images. Three PO trajectories [sequential, center-out, and interleaved (Fig. 1)], and two segment interpolation methods [nearest neighbor (NN) and linear interpolation (LI) (Fig. 2)] are most widely used. This study was performed to quantify the ghost intensity, signal-to-noise ratio (SNR), tag blurring, and the displacement of the myocardial tags on computer-simulated images and cine gradient echo MRI scans performed on a deformable phantom and the LV in a human volunteer.

METHODS

Computer Simulations

Simulations of fast gradient-echo (*fgre*) segmented k-space cine scans were performed on a Sun workstation (Sun Microsystems, Mountain View, CA) using Interactive Data Language (Research Systems, Boulder, CO). A reference gold standard nonsegmented image series of 120 frames was created which consisted of a horizontal bar of seven pixels in width moving in a sinusoidal cyclical fashion along a vertical path over a distance of 12.8 pixels at a rate of 0.4 pixels per image. This movement approximates a 0.4 mm displacement of the LV wall in 12 msec, a typical repetition time used in cine gradient echo imaging. The pixel intensity of the bar was 150 units and the background was 75 units. Rows of the Fourier transforms of the images (k-space rows) were extracted to simulate *fgre* segmented k-space acquisitions using sequential, center-out, and interleaved POs. The acquisitions were simulated at two, four, six, and

eight views per segment (VPS). The maximum number of view-shared images (VPS-1 intermediate images) was reconstructed using the NN and LI interpolation methods. Quantitative measurements of maximum ghost intensity, extent of total distance traveled, and the full-width half-maximum (FWHM) of the bar during maximum velocity were made.

Phantom Experiments

A deformable phantom was constructed by filling a balloon with firm gelatin and placing it in a box against a flat plate connected by a rigid rod to a cam on a motor placed at the foot of the MRI scan table. The gelatin was prepared as 56 gm/L of gelatin (Knox Co., Parsippany, NJ) in distilled water with a resultant T1 of 2300 msec and a T2 of 600 msec. The motor rotated at 52 cycles/min, and as it rotated, the plate deformed the balloon by approximately 5 mm per cycle. With every cycle of the cam, a light emitting diode (LED) was activated that in turn triggered the MR scan acquisition via peripheral gating.

The MRI scans were performed on a 1.5 T Signa CV/i scanner (GE Medical Systems, Waukesha, WI) using the body coil. Image reconstruction was performed with two methods: (a) a prospectively gated, NN reconstructed scanning sequence (*fastcard*, G.E. Medical Systems), and (b) a retrospectively gated, LI reconstructed sequence (*fastcine*, GE Medical Systems). Since *fastcine* is retrospectively gated (phases are acquired throughout the end of the cardiac cycle) and *fastcard* has a trigger window of 10% of the cardiac cycle in which no phases are acquired (to ensure the gating trigger is found for the next cycle), the *fastcard* scan was acquired first and then approximately 10% more phases were prescribed for the *fastcine* scan in order to achieve the same temporal resolution. Scans were performed using two-dimensional DANTE tags with six and eight VPS for each PO. The maximum view-shared images were reconstructed. A nonsegmented (one VPS) scan was acquired for each PO as the gold standard.

An 18 msec TR was chosen so that the relative amount of movement in our phantom would approximate a human heart with a heart rate of 75 beats per minute and a TR of 12 msec. Other imaging parameters included a 1.7 msec TE, full NEX and phase field of view (FOV), 1.25 mm × 1.25 mm pixel size, a 32 cm FOV, a 10 mm slice thickness, a 20° flip angle, and a bandwidth of ± 31 kHz.

The FWHM measurements were made on a tag in a midcontraction frame. All trials had tags applied at the same position, and measurements were made on the same

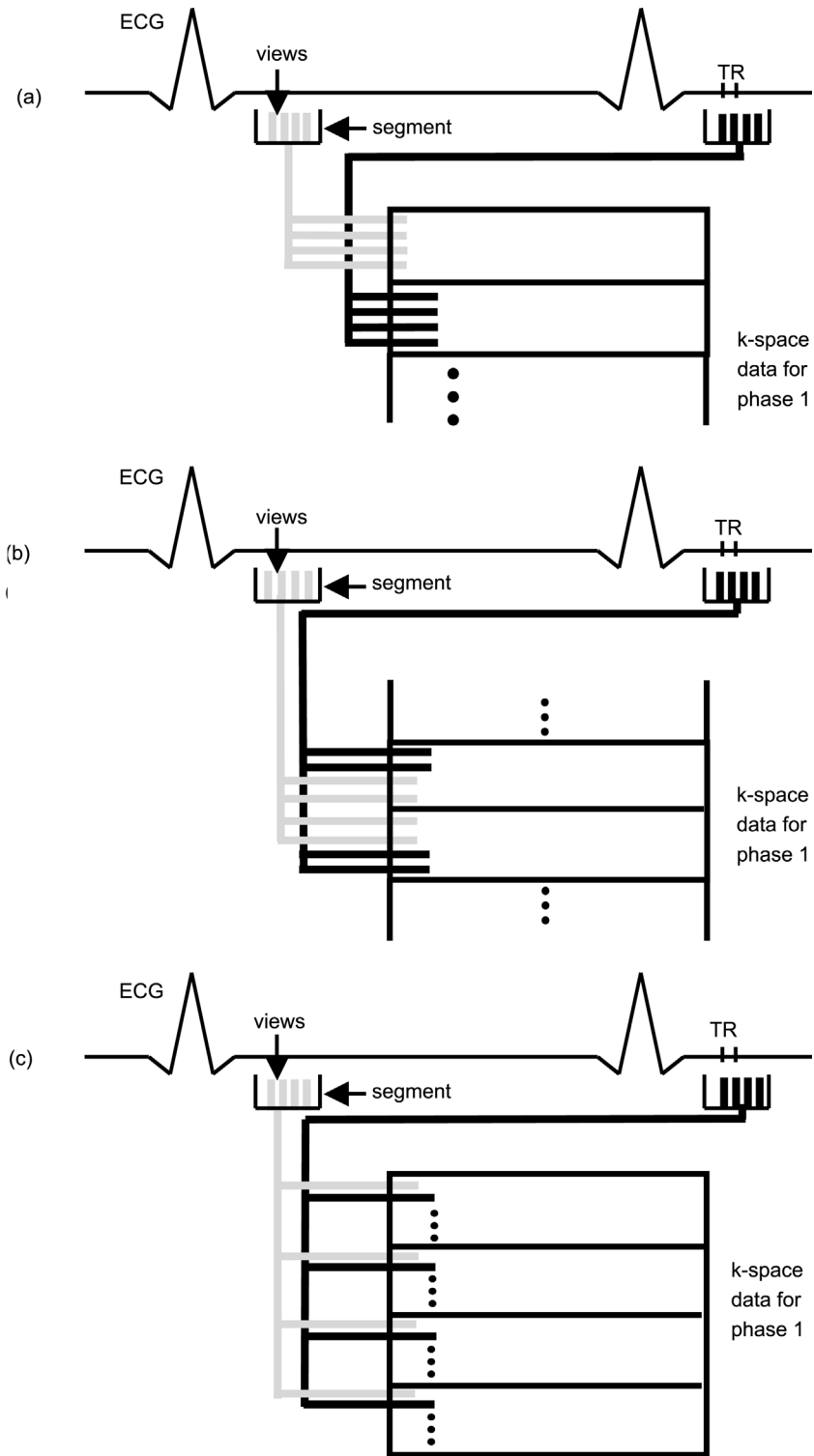


Figure 1. Three phase order acquisitions. This figure shows a four VPS acquisition. (a) Sequential scheme is either top-down or bottom-up. (b) Center-out scheme. The center lines of k-space are filled first and then alternating views move toward the edge of k-space until it is filled. (c) Interleaved PO scheme. k-space sampled uniformly during each segment. Each segment is interleaved until all of the k-space is filled.

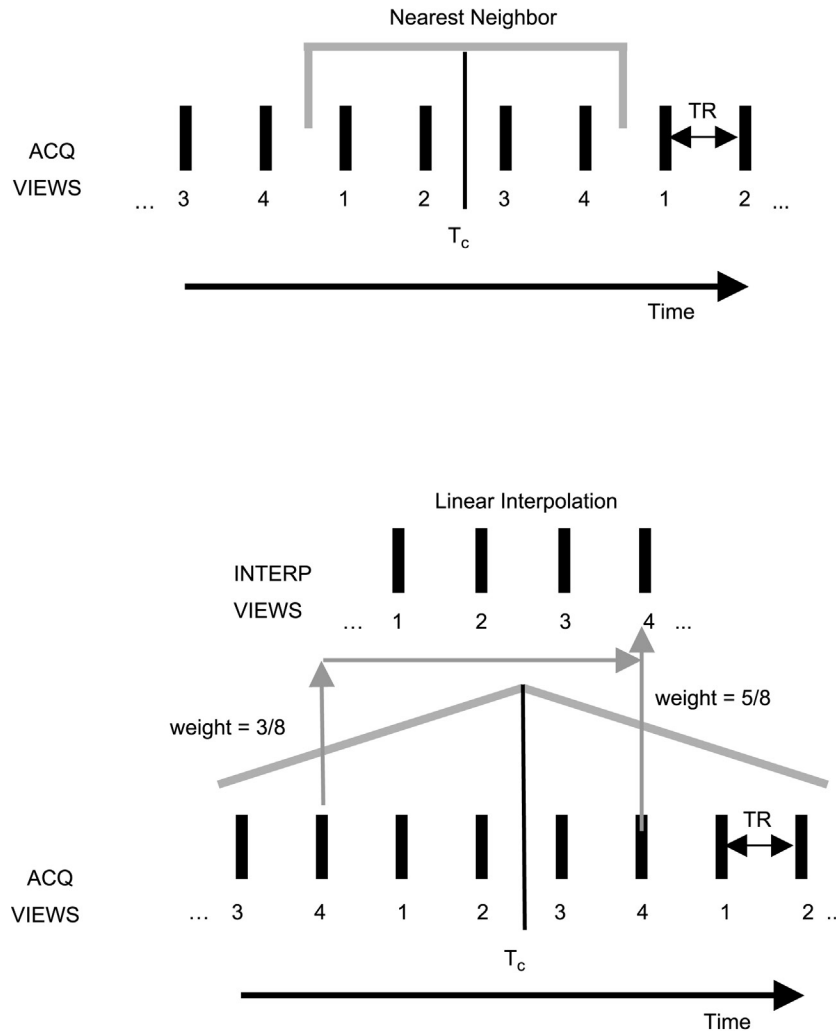


Figure 2. The NN (top) and LI (bottom) for a four VPS acquisition. Images reconstructed with the NN interpolation filter consist of the acquired views that lie closest to the frame's center time (T_c). This forms a rectangular window with a temporal width of $VPS \cdot TR$. The LI technique uses a triangular window with a temporal width of $2 \cdot VPS \cdot TR$. Each LI view is a weighted average of two views separated by the $VPS \cdot TR$. The weight is inversely proportional to the view's distance from T_c .

tag segment at the same time delay from the gating trigger. Tag displacement was tracked throughout contraction and relaxation using an intersection of the two-dimensional tags. Tag intersections were determined manually with a zoom factor of eight. Noise standard deviation was measured in a large region of interest (ROI) in the background of the image where no ghosting occurred. The average signal intensity within a ROI, including the image ghosts, was compared to the average signal intensity within a similar background region where no ghosting was present. The average of these intensities for all the images were then expressed as a ratio.

In Vivo Experiments

After informed consent was obtained in accordance to our institution's investigational review board, a standard short-axis scan of the LV of a single volunteer was performed. All scans were breath-held and a phased-array cardiac coil was used. The TR was 10.6 msec for the *fastcard* and nonsegmented scans and 10.2 msec for the *fastcine* scans. The TE was 5.7 msec for all scans. Other scan parameters included full NEX and phase FOV, $0.9375 \text{ mm} \times 0.9375 \text{ mm}$ pixel size, a 24 cm FOV, a 8-mm slice thickness, a 10° flip angle, and a bandwidth

of ± 31 kHz. Measurements of tag displacement and FWHM were made in the same manner as the phantom scan measurements.

RESULTS

Simulation

The simulation results for the eight VPS acquisition are summarized in Table 1. All FWHM measurements are made on a frame where the velocity of the bar is the highest midway between the cycle extremes. The residual sum of squares confirms the observation of jerky apparent motion with interleaved phase order. The nonsegmented image had a FWHM of 7.3 pixels so there was no significant blurring for any of the scans. The ghost intensity value is given as the increase over the constant background value. The extent of a full cycle that each bar traveled is measured by the movement of the peak intensity of the bar. A midcycle image for each PO and interpolation method and displacement of the peak value of the bar through a linear portion of the cyclic motion is shown in Fig. 3.

Phantom

Figure 4 shows the balloon gel phantom for an eight VPS acquisition for both interpolation methods and all POs. The plate is against the lower left corner, where the greatest deformation takes place. An intersection of tags in that area [shown in Fig. 4 (i)] is tracked over the deformation cycle and a graph of these results for each

PO is shown. The FWHM measurements made on the horizontal (perpendicular to the frequency encode direction) and vertical (perpendicular to the phase encode direction) tags marked in Fig. 4 (ii and iii) are summarized in Table 2. All LI tags except the vertical sequential are within one half pixel of the nonsegmented FWHM, whereas the NN tags have a greater variability.

The standard deviation of the background noise is reduced in the LI images relative to the NN images for all PO cases: 19% reduction in sequential, 18% in center-out, and 14% in interleaved. Ghosting severity is worst in the sequential PO scan, moderate in the center-out, and virtually imperceptible in the interleaved scan. Table 2 lists the average ghost intensity percent increase over the background value. The LI center-out PO is rated the highest and is considerably better than the NN center-out PO images; the interleaved PO pair is second best, and the sequential PO LI and NN scans display the poorest quality. The long T1 of the gelatin (2300 msec) produces greater ghosting than is typically observed in vivo; however, the relative amount of ghosting of each PO and interpolation method should be maintained.

In Vivo

The short-axis view of the volunteer's LV for an eight VPS acquisition for both interpolation methods and all POs is shown in Fig. 5. As in the phantom, the intersection of tags shown in Fig. 5 (i) was tracked over the first half of the cardiac cycle. Although care was taken to image the heart in the same position, the intrinsic variability in in vivo breath-held measurements make

Table 1

Simulation Results for Eight VPS Acquisition

		Sequential	Center-Out	Interleaved
Residual sum of squares	NN	18.6	14.8	80.8
	LI	17.8	17.7	67.1
Extent of cycle	NN	93%	93%	93%
	LI	89%	89%	93%
FWHM (pixels) ^a	NN	7.3	7.3	7.1
	LI	7.5	7.5	7.3
Ghost increase over background	NN	12%	5%	11%
	LI	5%	4%	5%

^aThe FWHM of bar in noninterpolated reconstruction is 7.3 pixels.

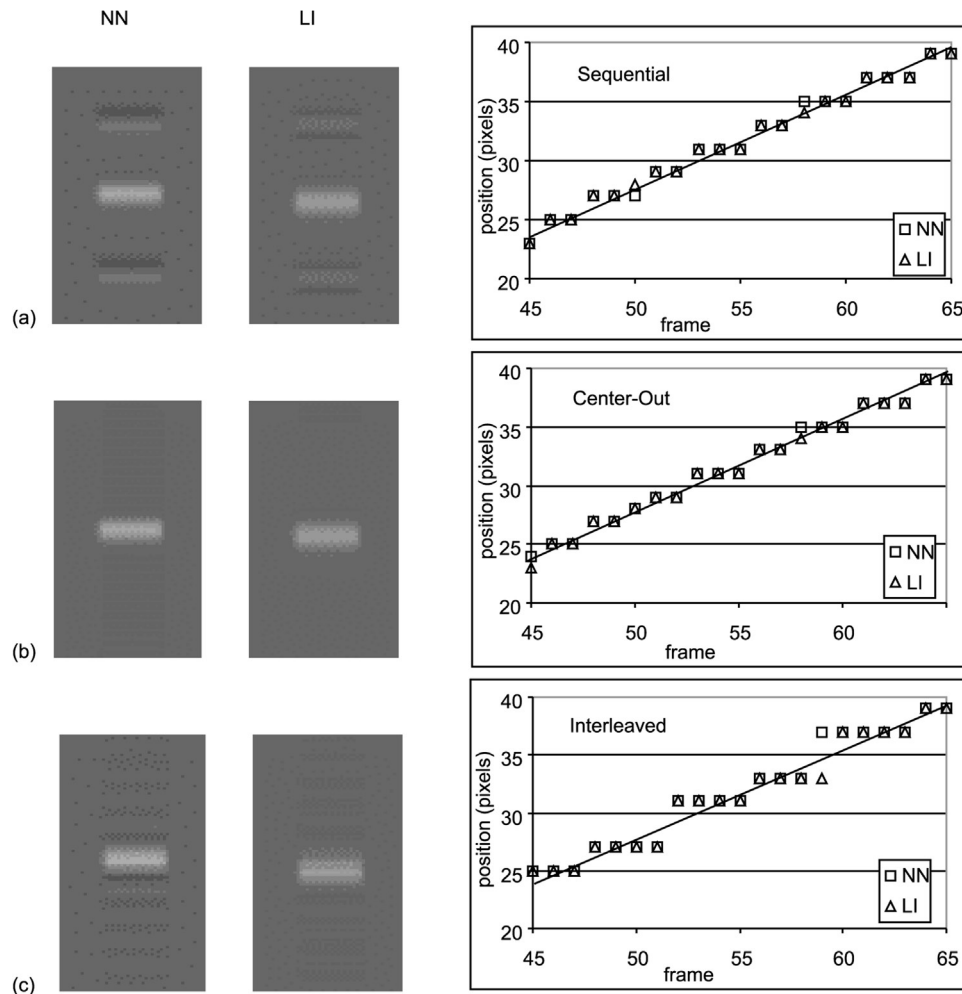


Figure 3. Simulated eight VPS acquisition of bar in midcycle motion for (a) sequential, (b) center-out, and (c) interleaved POs. Subjectively, the center-out PO has the best image quality. The corresponding displacement plots during a linear portion of the simulation cycle demonstrates that the interleaved PO provides less accurate tracking of the motion.

Table 2

Phantom Scan Results for Eight VPS Acquisition

		Sequential	Center-Out	Interleaved
Horizontal FWHM (pixels) ^a	NN	5	4	3
	LI	2.5	2.5	3.5
Vertical FWHM (pixels)	NN	4	2	1.5
	LI	1	2	3
Ghost increase over background	NN	65%	56%	22%
	LI	46%	36%	19%

^aThe FWHM of nonsegmented scans are 3 pixels for horizontal tags and 2.5 pixels for vertical tags, and ghost increase over background is 19%.

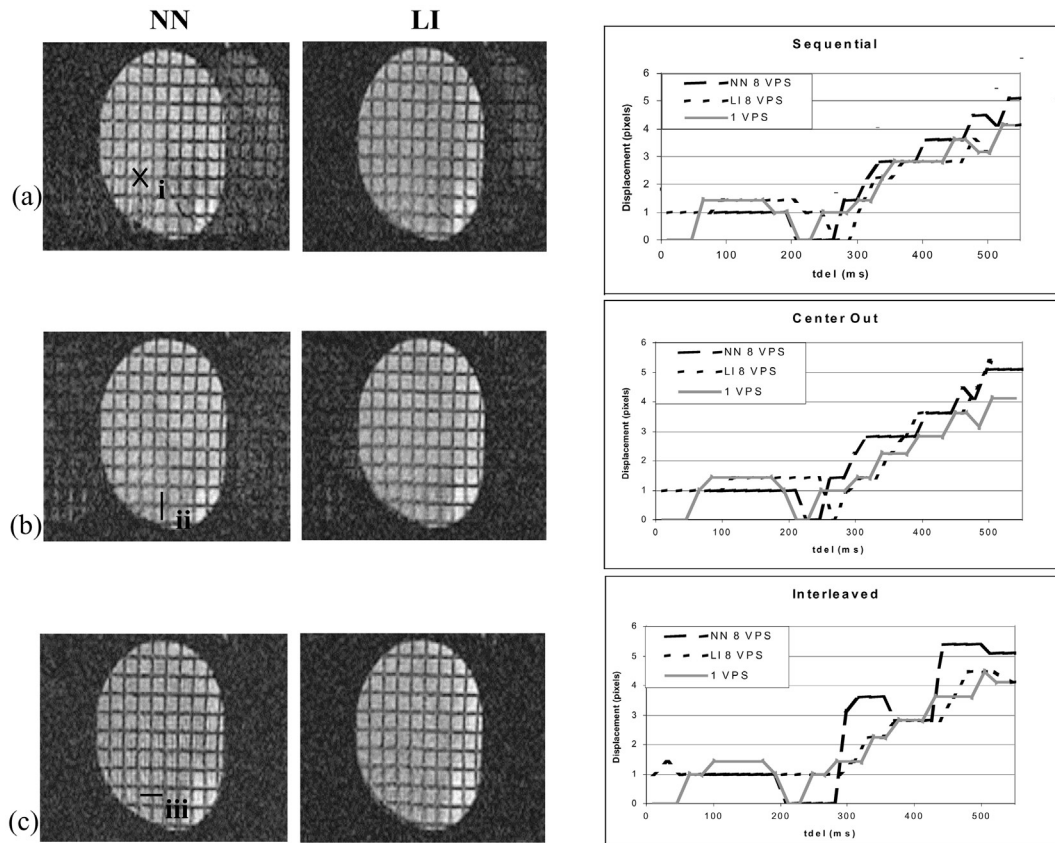


Figure 4. Balloon gel phantom with an eight VPS acquisition for (a) sequential, (b) center-out, and (c) interleaved POs. Subjectively, in each PO pair the LI scan is rated as having better image quality. Displacement curves, tracking the motion of marker *i* during phantom deformation, are shown on the right. In the interleaved PO, the NN tracking is highly erratic. Markers *ii* and *iii* denote positions used for full-width half-maximum measurements. Frequency encode direction is top-to-bottom in all images.

interpretation of these results more difficult. Slight changes in position, valsalva pressure, and heart rate are recognized variables. However, all displacement trajectories except in the NN sequential PO scan measured within two pixels of the averaged nonsegmented scan displacement trajectory. The discrepancy in the NN sequential PO scan is most likely caused by the difficulty in determining the tag intersection due to the poor image and tag quality.

The NN scans for all PO exhibit poor tag definition, with the sequential PO being the most difficult to analyze. Table 3 shows the FWHM measurements made on the tags marked in Fig. 5 (i and ii). The standard deviation of the background noise was reduced 15% in the LI images relative to the NN images for all PO cases.

The ghosting in vivo is imperceptible in all scans and therefore is not assessed.

DISCUSSION

The results for the simulation, phantom, and in vivo tag experiments are consistent in that image quality is reliably high for LI center-out PO scans, and the tag appearance and position are equivalent to the sequential PO. The center-out PO images have only one TR separating the center-lines of k-space, which contributes to the superior image quality. Each of the center groups contains half of the views acquired during one segment, with the remaining views in the symmetric group.

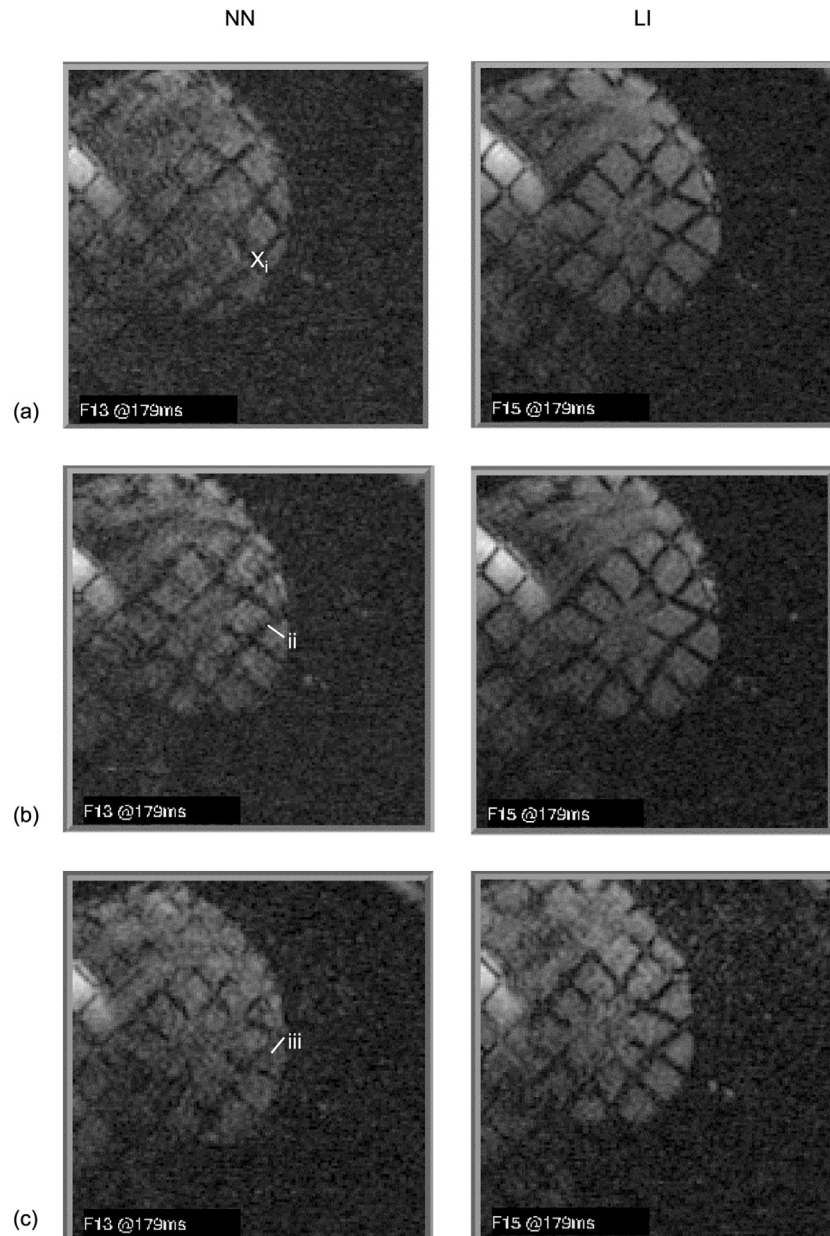


Figure 5. Scan of the short axis of a left ventricle acquisition for (a) sequential, (b) center-out, and (c) interleaved POs. Visually, the LI scans provide sharper tags; center-out and sequential PO scans have the best defined tags, whereas the interleaved PO tags are less distinct. Marker i denotes the tag intersection used for displacement measurements and markers ii and iii denote positions used for full-width half-maximum measurements. Frequency encode direction is top-to-bottom in all images.

A problem that occurs with the interleaved PO when view-sharing (either NN or LI) is implemented has been described in the context of phase-contrast imaging (13). Because the temporally uniform segments surround the center of k-space, the intermediate views are weighted toward one acquired image while more than half of the

views from that image contribute to the intermediate image. When the weighting shifts, the intermediate image then closely resembles the next acquired image. In tagged images, this results in a nonfluid cine reconstruction that inaccurately represents the intermediate frames. Therefore, view-shared interleaved PO scans should not

Table 3
Heart Scan Results for Eight VPS Acquisition

		Sequential	Center-Out	Interleaved
L-R FWHM [Fig. 5(ii)] (pixels)	Non	4.9	4.0	4.1
	NN	2.9	3.8	2.7
	LI	4.0	4.4	3.6
R-L FWHM [Fig. 5(iii)] (pixels)	Non	2.9	2.7	2.5
	NN	5.8	6.3	3.3
Ghost increase over background	LI	2.7	4.2	4.3

be used; the nonfluid motion results in displacement measurements that may be incorrect by more than a pixel. These errors will increase as the VPS and the object velocity increase. Optimum tag definition will be achieved when tag lines are perpendicular to the frequency encoding direction (3).

The frequency response (14) and phase-contrast effects (15) of the NN and LI filters have been investigated previously, but the results were not extended to myocardial tags. The NN filter has a better pass-band response, while the LI filter acts like a low-pass filter, which could blur the high-frequency tags, although this proved not to be severe. In addition, better LI stop-band response was shown to reduce ghosting. The LI technique improves the qualitative appearance and the SNR of cardiac images due to the averaging effects of the filter (16). Higher orders of interpolation introduce more noise and increase the temporal window and, thus, were not considered (15,17).

The results of this study are limited to patients with a regular heart rhythm and to those whose heart rate allows the acquisition of adequate nonview-shared frames. In addition, this work compared the NN and LI segment interpolation methods at the temporal resolution of the NN scans. The LI prescription allows the user to choose the number of frames reconstructed for a scan, and the analysis cannot be directly applied if a different temporal resolution is selected.

In conclusion, it is recommended that all tagged images be acquired with center-out phase order and reconstructed with the LI method to achieve the best appearance and positional accuracy. The other acquisition orders and segment interpolation techniques used during reconstruction may introduce errors in determining tag placement for myocardial position or thickness measurements. This type of error could lead to incorrect diagnosis of myocardial ischemia or viability.

ABBREVIATIONS

LI	linear interpolation
NN	nearest neighbor
PO	phase encode order
SNR	signal-to-noise ratio
VPS	views per segment

REFERENCES

1. Reichek, N. Myocardial Tagging. *J. Magn. Reson. Imaging* **1999**, *10*, 609–616.
2. Axel, L.; Dougherty, L. MR Imaging of Motion with Spatial Modulation of Magnetization. *Radiology* **1989**, *171*, 841–845.
3. McVeigh, E.R. MRI of Myocardial Function: Motion Tracking Techniques. *Magn. Reson. Imaging* **1996**, *14* (2), 137–150.
4. Zerhouni, E.A.; Parish, D.M.; Rogers, W.J.; Yang, A.; Shapiro, E.P. Human Heart: Tagging with MR Imaging—A Method for Noninvasive Assessment of Myocardial Motion. *Radiology* **1988**, *169*, 59–63.
5. Clark, N.R.; Reichek, N.; Bergey, P.; Hoffman, E.A.; Brownson, D.; Palmon, L.; Axel, L. Circumferential Myocardial Shortening in the Normal Human Left Ventricle. *Circulation* **1991**, *84*, 67–74.
6. Lombardo, A.; Loperfido, F.; Trani, C.; Pennestrì, F.; Rossi, E.; Giordano, A.; Possati, G.; Maseri, A. Contractile Reserve of Dysfunctional Myocardium After Revascularization: A Dobutamine Stress Echocardiography Study. *J. Am. Coll. Cardiol.* **1997**, *30*, 633–640.
7. Iwado, Y.; Mizushige, K.; Watanabe, K.; Ueda, T.; Furumoto, W.; Nozaki, S.; Sakamoto, S.; Ohmori, K.; Matsuo, H. Quantitative Analysis of Myocardial Response to Dobutamine by Measurement of Left Ventricular Wall Motion Using Omnidirectional

- M-Mode Echocardiography. *Am. J. Cardiol.* **1999**, *83*, 765–769.
8. Kramer, C.M.; Lima, J.A.; Reichek, N.; Ferrari, V.A.; Llaneras, M.R.; Palmon, L.C.; Yeh, I.T.; Tallant, B.; Axel, L. Regional Differences in Function Within Noninfarcted Myocardium During Left Ventricular Remodeling. *Circulation* **1993**, *88* (3), 1279–1288.
 9. Sayad, D.E.; Willett, D.L.; Hundley, W.G.; Grayburn, P.A.; Peshock, R.M. Dobutamine Magnetic Resonance Imaging with Myocardial Tagging Quantitatively Predicts Improvement in Regional Function After Revascularization. *Am. J. Cardiol.* **1998**, *82* (9), 1149–1151.
 10. McVeigh, E.R.; Atalar, E. Cardiac Tagging with Breath-Hold Cine MRI. *Magn. Reson. Med.* **1992**, *28*, 318–327.
 11. Atkinson, D.J.; Edelman, R.R. Cineangiography of the Heart in a Single Breath Hold with a Segmented TurboFLASH Sequence. *Radiology* **1991**, *178*, 357–360.
 12. Foo, T.K.F.; Bernstein, M.A.; Aisen, A.M.; Hernandez, R.J.; Collick, B.D.; Bernstein, T. Improved Ejection Fraction and Flow Velocity Estimates with Use of View Sharing and Uniform Repetition Time Excitation with Fast Cardiac Techniques. *Radiology* **1995**, *195*, 471–478.
 13. Polzin, J.A.; Frayne, R.; Grist, T.M.; Mistretta, C.A. Frequency Response of Multi-phase Segmented k-Space Phase-Contrast. *Magn. Reson. Med.* **1996**, *35*, 755–762.
 14. Parker, J.A.; Kenyon, R.V.; Troxel, D.E. Comparison of Interpolation Methods for Image Resampling. *IEEE Trans. Med. Imaging* **1983**, *MI-2* (1), 31–39.
 15. Frayne, R.; Rutt, B.K. Frequency Response of Retrospectively Gated Phase-Contrast MR Imaging: Effect of Interpolation. *J. Magn. Reson. Imaging* **1993**, *3*, 907–917.
 16. Epstein, F.H.; Arai, A.E.; Hartley, M.R.; Wolff, S.D. Improved Appearance of Segmented k-Space Fast Gradient-Echo Cardiac Images by Interpolated Reconstruction (Abstr). *Proceedings of the Society of Magnetic Resonance in Medicine*; Society of Magnetic Resonance in Medicine: Vancouver, B.C., 1997; 2011.
 17. Lenz, G.W.; Haacke, E.M.; White, R.D. Retrospective Cardiac Gating: A Review of Technical Aspects and Future Directions. *Magn. Reson. Imaging* **1989**, *7*, 445–455.

Received October 30, 2000

Accepted November 16, 2001